Modeling and Digital Suppression of Passive Nonlinear Distortion in Simultaneous Transmit–Receive Systems

Muhammad Zeeshan Waheed*†, Vesa Lampu†, Adnan Kiayani†, Marko Fleischer‡, Lauri Anttila†, and Mikko Valkama†

*Nokia Mobile Networks, Tampere, Finland
†Department of Electrical Engineering, Tampere University, Finland
‡Nokia Mobile Networks, Ulm, Germany
E-mail: muhammad.waheed@nokia.com

***Abstract*—In frequency division duplexing (FDD) based simultaneous transmit-receive systems, nonlinear behavior of the active and passive RF components can cause nonlinear distortion products falling at the receiver band. Such distortion may also arise over-the-air, if there are for example metallic objects in close vicinity of the antenna system. In this work, we focus on the modeling and digital cancellation of such distortion products, especially in case of passive harmonic distortion of the transmit waveform landing at the receiver band. We provide behavioral modeling of the problem, while also use the models to derive corresponding digital distortion cancellers. Practical RF measurement based numerical results are provided, focusing on a timely dual-band cellular transceiver scenario covering 5G NR bands n3 (1.8 GHz) and n78 (3.5 GHz). The RF measurement results demonstrate accurate modeling and distortion cancellation in the considered example cases.**

***Index Terms*—5G, carrier aggregation, duplexing, interference cancellation, nonlinear systems, passive intermodulation, passive harmonic distortion, simultaneous transmission and reception.**

I. Introduction

To support higher peak data rates and improved cell coverage, carrier aggregation (CA) technique was introduced in long term evolution (LTE)-Advanced Release 10, and is also included in 5G new radio (NR) standard. CA allows addition of multiple frequency chunks, called component carriers (CCs), within or across frequency bands, thereby enabling an efficient use of licensed spectrum [1].

In frequency-division duplexing (FDD) networks where transmitter (TX) and receiver (RX) operate simultaneously but at different frequencies, the inter-modulation distortion (IMD) from nonlinear components along the transmit signal path is critical [2]–[4]. The spurious IMD products due to mixing of signals in a passive nonlinear components is referred to as passive inter modulation (PIM), and has also been recognized as a major concern for FDD radios. The presence of PIM in the uplink band results in the elevated receiver noise floor, leading to throughput degradation and impaired end-user experience. The physical mechanism causing PIM can be diverse, for example various passive components in a radio unit such as connectors, combiner, filter, cable assembly, as well as rusty metallic objects in the close vicinity of the antenna can all contribute to PIM generation. The PIM due to rusty metallic objects in antenna near field is referred to as "rusty-bolt" effect, where it can also affect neighboring cells operating on the same site [5].

In practice, PIM can be avoided through proper frequency planning, however, such planning becomes impractical with the growing number of configured bands in a same radio or on a co-located site with FDD and TDD radios. The self-interference issue in FDD transceivers has been acknowledged and reported in several 3GPP CA related documents, such as [6] [7], which have also proposed some alternatives to mitigate its impact. These include, for example, to apply the maximum power reduction (MPR) – to reduce the strength of the interference – or the maximum sensitivity degradation (MSD) – to enhance the receiver sensitivity. However, the adoption of such approaches lead to reduction in cell coverage and throughput loss. Advanced digital cancellation techniques have recently been proposed that exploit the fact that the interference can be regenerated in the receiver digital front-end and removed by subtracting the model output from the actual received signal [8]–[10].

In this paper, we expand our previous work in [11] and [12] on digital self-interference cancellation, but now focus on passive harmonic (PHM) distortion that couples over the air. Furthermore, the proposed framework for digital cancellation now assumes a multiple-input-multiple-output (MIMO) FDD radio setup. The proposed digital cancellation method is tested and verified through practical RF measurements assuming co-existing 5G NR band N3 FDD and band N78 TDD operation, where the second-order passive harmonic distortion of band N3 lands within the receiver band of the band N78, as shown in Fig. 1. The rest of the paper is organized as follows. In Section II, we address baseband equivalent model of PHM distortion generated at RX band by external sources in the antenna near field and the relevant digital cancellation methods and parameter estimation procedures. In section III, the performance of the proposed digital cancellation method is evaluated with practical radio frequency (RF) measurements. Finally, Section IV concludes the paper.

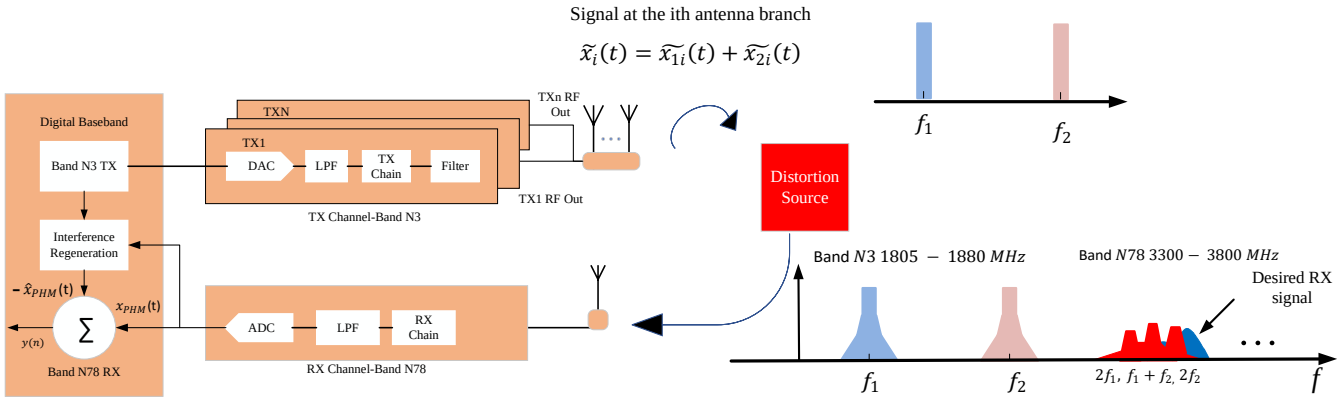

Fig. 1. Simplified block diagram of the considered setup showing modeling-related notations and spectral illustration of the second-order passive harmonic distortion that is created by passive metallic objects in the antenna near field, appearing in one of the configured RX bands.

II. Passive Harmonic Distortion: Modeling and Proposed Digital Cancellation Methods

We begin by formulating the self-interference problem, assuming a MIMO FDD system and air-induced passive harmonic distortion (PHM) that couples into a co-located TDD radio. Building on the proposel signal modeling, we then develop a linear-in-parameters model for digital estimation and cancellation.

A. Self-Interference Model

We consider a generic MIMO-FDD transceiver, as shown in Fig 1, where the transmitter has N transmit antennas and employs carrier aggregation with two CCs. The up-converted I/Q modulated CC signals from $i-$th transmitter are given as

$$\begin{aligned}\tilde{x}_{1i} &= \mathrm{Re}\{\alpha_{1i}x_{1i}e^{j\omega_1 n}\}\\ \tilde{x}_{2i} &= \mathrm{Re}\{\alpha_{2i}x_{2i}e^{j\omega_2 n}\},\end{aligned} \tag{1}$$

where x_{1i} and x_{2i} are the two CCs in the baseband, α_1 and α_2 represent the complex gains, and ω_1 and ω_2 are center-frequency of the corresponding CCs after up-conversion. It is noted that the up-converted I/Q modulated CC signals are continuous-time in an actual system. However, this does not impact the accuracy of the modelling since we consider the center frequencies of the CCs only in order to determine where the resulting nonlinear terms will fall in the frequency domain.

In practice, the components carriers may belong to the same RF band (intra-band CA) or can be aggregated across different bands (inter-band CA). For the latter case, the RF CC signals may be combined after the PA in a diplexer when they have a separate TX/RX line-up or before a *multi-band PA* if the RF spacing between the bands is small. For notational simplicity, we assume in this paper intra-band CA scenario and restrict our focus to only two CCs; nevertheless, the proposed modeling is applicable to inter-band CA as well since the PHM distortion source is assumed to be outside the radio. The aggregated TX signal of the $i-$th antenna branch is then a sum of all CC signals, i.e., $\tilde{x}_i(t) = \tilde{x}_{1i}(t) + \tilde{x}_{2i}(t)$.

The signal from all transmit antenna branches propagate and are incident on a PHM distortion source, which is assumed to be in close proximity of antenna unit. Using a polynomial model, the signal after static PHM nonlinearity is given by

$$\begin{aligned}\tilde{x}_{PHM}(t) &= \sum_{p=1}^{P}\beta_p.(\sum_{i=1}^{N}\tilde{x}_i(t)))^p\\ &= \sum_{p=1}^{P}\beta_p.\{\mathrm{Re}\{(\alpha_{11}x_{11}(t)+\alpha_{12}x_{12}(t)+.....+\alpha_{1N}x_{1N}(t))e^{j\omega_1 n}\}\\ &+\mathrm{Re}\{(\alpha_{21}x_{21}(t)+\alpha_{22}x_{22}(t)+.....+\alpha_{2N}x_{2N}(t))e^{j\omega_1 n}\}\}^p\\ &= \sum_{p=1}^{P}\beta_p\{\mathrm{Re}\{\psi_1(t)e^{j\omega_1 n}\}+\mathrm{Re}\{\psi_2(t)e^{j\omega_2 n}\}\}^p\end{aligned} \tag{2}$$

where

$$\begin{aligned}\psi_1(t) &= \sum_{i=1}^{N}\alpha_{1,i}x_{1,i}(t)\\ \psi_2(t) &= \sum_{i=1}^{N}\alpha_{2,i}x_{2,i}(t).\end{aligned}$$

Now using the identities of the form

$$\mathrm{Re}\{ue^{jv}\} = 1/2(ue^{jv}+u^*e^{-jv}), \tag{3}$$

and

$$(u+v)^p = \sum_{k=0}^{p}\binom{p}{k}u^k v^{p-k}, \tag{4}$$

we expand the expression in (2) which yields

$$\begin{aligned}\tilde{x}_{PHM}(t) &= \sum_{p=1}^{P}\beta_p\times\\ &\sum_{k=0}^{p}\binom{p}{k}\frac{1}{2^k}\sum_{k_1=0}^{p}\binom{k}{k_1}\psi_1^{k_1}e^{jk_1\omega_1 t}(\psi_1^*)^{k-k_1}e^{j(k-k_1)\omega_1 t}\times\\ &\frac{1}{2^{p-k}}\sum_{k_2=0}^{p-k}\binom{p-k}{k_2}\psi_2^{k_2}e^{jk_2\omega_2 t}(\psi_2^*)^{p-k-k_2}e^{j(k+k_2-p)\omega_2 t}.\end{aligned} \tag{5}$$

TABLE I
INSTANTANEOUS BASIS FUNCTIONS FOR $p = 2$ AND $p = 4$

Value of p	**Basis functions,** $2\omega_1$	**Basis functions,** $2\omega_2$	**Basis functions,** $\omega_1 + \omega_2$
2	$x_{11}^2,\, x_{12}^2, x_{11}x_{12}$	$x_{21}^2,\, x_{22}^2, x_{21}x_{22}$	$x_{11}x_{21},\, x_{11}x_{22},\, x_{12}x_{21},\, x_{12}x_{22}$
4	$x_{11}^2,\, x_{12}^2, x_{11}x_{12},\, x_{11}^3x_{11}^*,\, x_{11}^3x_{12}^*,$ $x_{11}^2x_{12}x_{11}^*,\, x_{11}^2x_{12}x_{12}^*,\, x_{12}^2x_{11}x_{11}^*,$ $x_{12}^2x_{11}x_{12}^*,\, x_{12}^3x_{11}^*,\, x_{12}^3x_{12}^*,$ $x_{11}^2x_{12}x_{11}^*,$ $x_{11}^2x_{12}x_{12}^*,\, x_{11}x_{12}^2x_{11}^*,\, x_{11}x_{12}^2x_{12}^*,$ $x_{11}^2x_{21}x_{21}^*,\, x_{11}^2x_{21}x_{22}^*,\, x_{11}^2x_{22}x_{21}^*,$ $x_{11}^2x_{22}x_{22}^*,$ $x_{12}^2x_{21}x_{21}^*,\, x_{12}^2x_{21}x_{22}^*,\, x_{12}^2x_{22}x_{21}^*,$ $x_{12}^2x_{22}x_{22}^*,\, x_{11}x_{12}x_{21}x_{21}^*,$ $x_{11}x_{12}x_{21}x_{22}^*,\, x_{11}x_{12}x_{22}x_{21}^*,$ $x_{11}x_{12}x_{22}x_{22}^*$	$x_{21}^2,\, x_{22}^2, x_{21}x_{22},\, x_{21}^2x_{11}x_{11}^*,$ $x_{21}^2x_{11}x_{12}^*,\, x_{21}^2x_{12}x_{11}^*,\, x_{21}^2x_{12}x_{12}^*,$ $x_{22}^2x_{11}x_{11}^*,\, x_{22}^2x_{11}x_{12}^*,\, x_{22}^2x_{12}x_{11},$ $x_{22}^2x_{12}x_{12}^*,\, x_{21}x_{22}x_{11}x_{11}^*,$ $x_{21}x_{22}x_{11}x_{12}^*,$ $x_{21}x_{22}x_{12}x_{11}^*,\, x_{21}x_{22}x_{12}x_{12}^*,$ $x_{21}^2x_{21}x_{21}^*,$ $x_{21}^2x_{21}x_{22}^*,\, x_{21}^2x_{22}x_{21}^*,\, x_{21}^2x_{22}x_{22}^*,$ $x_{22}^2x_{21}x_{21}^*,\, x_{22}^2x_{21}x_{22}^*,\, x_{22}^2x_{22}x_{21}^*,$ $x_{22}^2x_{22}x_{22}^*,\, x_{21}x_{22}x_{21}x_{21}^*,$ $x_{21}x_{22}x_{21}x_{22}^*,$ $x_{21}x_{22}x_{22}x_{21}^*,\, x_{21}x_{22}x_{22}x_{22}^*$	$x_{11}x_{21},\, x_{11}x_{22},\, x_{12}x_{21},\, x_{12}x_{22},$ $x_{11}x_{11}^*x_{11}x_{21},\, x_{11}x_{11}^*x_{11}x_{22},$ $x_{11}x_{11}^*x_{12}x_{21},\, x_{11}x_{11}^*x_{11}x_{22},$ $x_{11}x_{12}^*x_{11}x_{21},$ $x_{11}x_{12}^*x_{11}x_{22},\, x_{11}x_{12}^*x_{12}x_{21},\, x_{11}x_{12}^*x_{12}x_{22},$ $x_{12}x_{11}^*x_{11}x_{21},\, x_{12}x_{11}^*x_{11}x_{22},\, x_{12}x_{11}^*x_{12}x_{21},$ $x_{12}x_{11}^*x_{12}x_{22},\ x_{12}x_{12}^*x_{11}x_{21},\, x_{12}x_{12}^*x_{11}x_{22},$ $x_{12}x_{12}^*x_{12}x_{21},$ $x_{12}x_{12}^*x_{11}x_{21},\, x_{12}x_{12}^*x_{12}x_{22},\, x_{21}x_{21}^*x_{11}x_{21},$ $x_{21}x_{21}^*x_{11}x_{22},\, x_{21}x_{21}^*x_{12}x_{21},\, x_{21}x_{21}^*x_{12}x_{22},$ $x_{21}x_{21}^*x_{11}x_{21},\, x_{21}x_{22}^*x_{11}x_{22},\, x_{21}x_{22}^*x_{12}x_{21},$ $x_{21}x_{22}^*x_{12}x_{22},$ $x_{22}x_{21}^*x_{11}x_{21},\, x_{22}x_{21}^*x_{11}x_{22},\, x_{22}x_{21}^*x_{12}x_{21},$ $x_{22}x_{22}^*x_{11}x_{21},$ $x_{22}x_{22}^*x_{11}x_{22},\, x_{22}x_{22}^*x_{12}x_{21},\, x_{22}x_{22}^*x_{12}x_{22}$

Resulting from (5), the PHM distortion with the basis functions (BFs) and their center frequencies is then given by

$$\begin{aligned}\tilde{x}_{PHM}(t) = \sum_{p=1}^{P}\sum_{k_1=0}^{p}\sum_{k_2=0}^{p-k}\gamma_{p,k_1,k_2}\times \\ \psi_1^{k_1}(\psi_1^*)^{k-k_1}\psi_2^{k_2}(\psi_2^*)^{p-k-k_2}\times \\ e^{j\left((2k_1-k)\omega_1+(2k_2+k-p)\omega_2\right)t}\end{aligned} \tag{6}$$

where, for notational simplicity, we have lumped all the scaling factors with the unknown complex PIM gain β_p and denote the overall effective coefficient as γ_{p,k_1,k_2}.

In this work, we are only interested in even-order passive harmonic distortion products, namely at frequencies $2\omega_1$, $2\omega_2$ and $\omega_1 + \omega_2$, which are likely to appear at the RX band in LTE-A and 5G FDD-TDD defined band combinations and also typically have high power to cause throughput degradation. The corresponding signals at these frequencies can be obtained by appropriately setting the value for the positive integers k_1 and k_2 in Equation (6). For instance, the signals at $2\omega_1$ can be obtained by imposing the following rules for the positive integers k_1 and k_2 in (6):

$$\begin{aligned} 2k_1 - k = 2 \qquad &\text{and} \quad 2k_2 + k - p = 0 \\ \rightarrow k_1 = \frac{1}{2}k + 1 \qquad &\text{and} \quad k_2 = \frac{1}{2}(p-k), \end{aligned}$$

where we can see that k_1 and k_2 needs to be integers, given that k and p must be even. Similar rules can be imposed for the BFs at $2\omega_2$ by setting

$$\begin{aligned} 2k_1 - k = 0 \qquad &\text{and} \quad 2k_2 + k - p = 2 \\ \rightarrow k_1 = \frac{1}{2}k \qquad &\text{and} \quad k_2 = 1 + \frac{1}{2}(p-k) \end{aligned}$$

and for the corresponding BFs at $\omega_1 + \omega_2$

$$\begin{aligned} 2k_1 - k = 1 \qquad &\text{and} \quad 2k_2 + k - p = 1 \\ \rightarrow k_1 = \frac{1}{2}(k+1) \qquad &\text{and} \quad k_2 = \frac{1}{2}(1+p-k). \end{aligned}$$

Finally, in order for k_1 and k_2 to be integers, the value of k must be adjusted accordingly, while p is always even. The value of k e.g., for the case $\omega_1 + \omega_2$ is set to 1.

For completeness of the modeling, the resulting nonlinear terms for $p = 2$ and $p = 4$ in a dual-band inter-CA scenario for all the three passive harmonic distortion frequencies are shown in Table I, where without loss of generality we drop the time-domain index (t) to shorten the notations.

Finally, the PHM distortion generated in a nonlinear passive source and sensed by a collocated radio is received together with the actual received signal of interest. The digital BB received signal after down-conversion and channel filtering is therefore given by

$$x_{BB}[n] = x_D[n] + \eta_{BB}[n] + x_{PHM}[n] \tag{7}$$

where $x_D[n]$ is the desired received signal and η_{BB} is additive noise.

B. Digital Cancellation and Parameter Estimation

The derived baseband signal models discussed in the previous section serve as the basis for the proposed digital PHM distortion canceller. The canceller specifically creates new PHM distortion samples using the basis functions from Table I, which are then subtracted from the actual received baseband signal.

The general assumption here is that the PHM is a nonlinear function of the transmit data that stems from the same site, and there's a single digital baseband unit with access to all aggressor and victim carriers, thus the PHM distortion can be digitally estimated and canceled in the digital baseband. The variables that serve as the complex weights of the basis function samples, or the equivalent model parameters, as denoted by γ_p in (6) are unknown and must thus be estimated.

Noting that Equation (6) is in fact a linear-in-parameters model, the parameter estimation can be carried out with linear least squares (LS). As a starting point, consider M samples of the observed baseband received signal $x_{BB}[n]$ in equation

(7) which, under observed PHM distortion, can be expressed as

$$\mathbf{x}_{BB} = \mathbf{\Phi}\boldsymbol{\gamma} + \mathbf{z}, \tag{8}$$

where $\mathbf{\Phi}$ is the nonlinear data matrix containing relevant basis functions that are constructed from the original TX data, $\boldsymbol{\gamma}$ denotes unknown coefficients that need to be estimated, and the desired received signal and noise in equation (6) are lumped into a single variable $\mathbf{z}$.

We shortly elaborate the structure of the matrix $\mathbf{\Phi}$ by restricting our focus to the example frequency of $2\omega_1$ and assuming $p = 2$, for which the instantaneous basis functions read as follows:

$$\begin{aligned} \phi_1[n] &= x_{11}^2[n] \\ \phi_2[n] &= x_{12}^2[n] \\ \phi_3[n] &= x_{11}[n]x_{12}[n]. \end{aligned} \tag{9}$$

Then, the nonlinear data matrix $\mathbf{\Phi}$ is obtained as follows:

$$\begin{aligned} &\mathbf{\Phi}[n] \\ &= \begin{bmatrix} \phi_1[n-M+1] & \phi_2[n-M+1] & \cdots & \phi_3[n-M+1] \\ \phi_1[n-M+2] & \phi_2[n-M+2] & \cdots & \phi_3[n-M+2] \\ \vdots & \vdots & \ddots & \vdots \\ \phi_1[n] & \phi_2[n] & \cdots & \phi_3[n] \end{bmatrix} \end{aligned} \tag{10}$$

and the parameter estimation is simply carried out as

$$\widehat{\boldsymbol{\gamma}} = \left(\mathbf{\Phi}^H[n]\mathbf{\Phi}[n]\right)^{-1}\mathbf{\Phi}^H[n]\mathbf{x}_{BB}[n] \tag{11}$$

where $\hat{\boldsymbol{\gamma}} = \begin{bmatrix}\widehat{\gamma}_1 & \widehat{\gamma}_2 & \widehat{\gamma}_3\end{bmatrix}^T$ contains the estimates for each coefficient, $(\cdot)^H$ denotes the Hermitian transpose, while $(\cdot)^T$ denotes the regular transpose.

Having estimated the coefficients using M observation samples, the actual cancellation performance can then be evaluated by regenerating the interference and then subtracting it from the received signal. In an online operation of the receiver, the received signal with interference cancellation is given by

$$y_c[n] = x_{BB}[n] - \mathbf{\Phi}[n]\hat{\boldsymbol{\gamma}}. \tag{12}$$

Next, in the following section, we analyze the accuracy and performance of our proposed digital cancellation methods with practical RF measurements. The measurement setup and results are presented and discussed.

III. RF Measurement Setup and Results

This section covers the description of the RF measurement setup utilized to evaluate the performance of the proposed digital cancellation method alongside the actual measured cancellation results.

A. Measurement Setup

The measurement setup is presented in Fig. 2. The measurements are conducted in an anechoic chamber with a true base-station hardware, where rusty metal and other similar test PHM distortion sources are also deployed at a distance of at least 1m from the base-station. The base-station hardware is controlled by a PC located outside the chamber to feed the input signals and to collect data from the base-station for post-processing. Furthermore, other relevant features of the measurement system and the digital canceller itself are show in Table II.

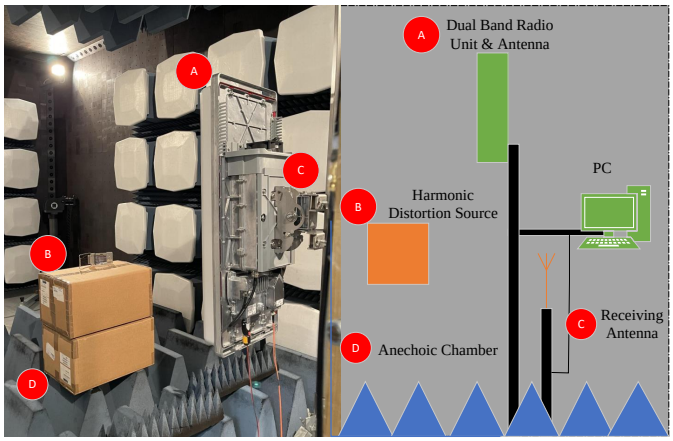

Fig. 2. Overall RF measurement setup used for evaluating the performance of the proposed digital cancellation method. Different parts of the system are also highlighted.

TABLE II
RF Measurement Setup Configuration and Considered PHM Distortion Canceller Parameters

Parameter	Value
Bandwidth of the CCs	5 MHz
Total transmit power	31 dBm
Center frequencies of CCs	1819.0/1866.5 MHz
RX center frequency	3685.0 MHz
RX capture bandwidth	122.8 MHz
Cancellation bandwidth	20 MHz
Signals per carrier frequencies	2
Polynomial order (P)	4
Number of samples used for estimation (N)	90 000

The base-station hardware comprises of a dual TX/RX system with directive antennas as show in Fig. 2 labeled as (A). The TX chains transmit two 5G NR standard-compliant CP-OFDM signals as CCs, with a bandwidth of 5 MHz and the transmit power being set to +31 dBm plus the antenna gain. In both the TX chains, each of the individual carriers lies at 5G NR band n3, at TX frequencies of 1819.0 MHz and 1866.5 MHz. The RX center frequency is set to 3685.0 MHz in the RX chain which correspond to the fundamental frequency of the 2nd passive harmonic distortion of the form $\omega_1 + \omega_2$. The data for post processing is utilized from the RX chain as indicated in Fig. 1.

The RX capture bandwidth is set to 122.8 MHz and the even-order harmonics at different frequencies are all captured at once which are then processed separately. The following section shows the cancellation results achieved for all the even-order harmonics, i.e., $\omega_1 + \omega_2$, $2\omega_1$, $2\omega_2$.

Furthermore, the proposed digital cancellation method considers polynomial order up to ($P = 4$), with the basis functions being shown in Table I. For the case of $2\omega_1$, there are a

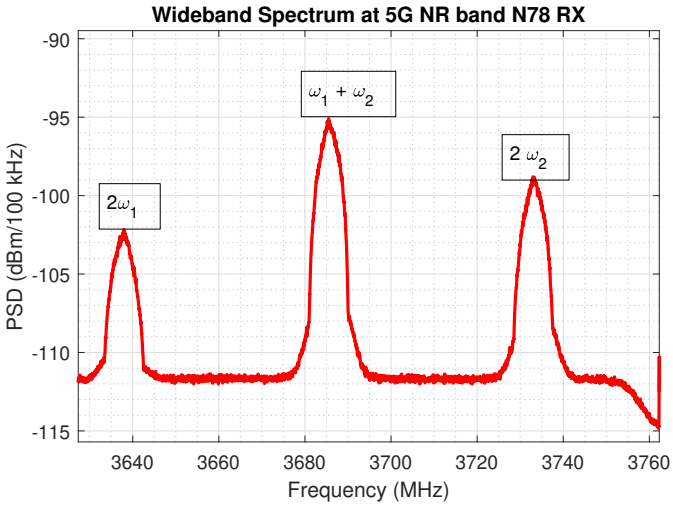

Fig. 3. Wideband spectrum of the observable PHM distortion at the RX band.

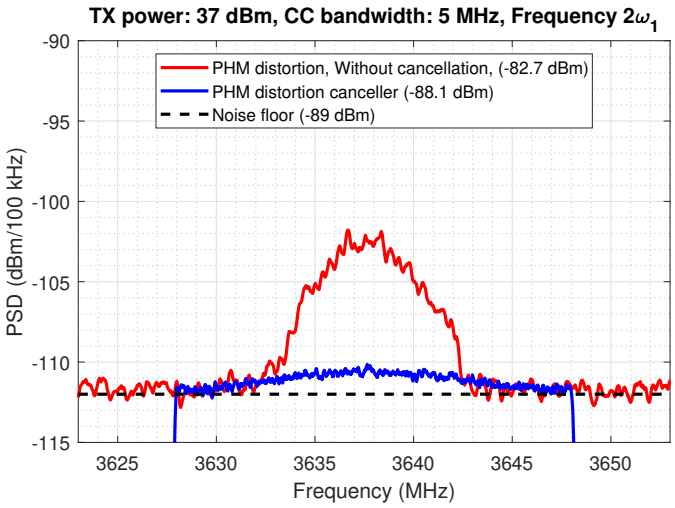

Fig. 4. The spectra of the observed PHM distortion at frequency $2\omega_1$ and the residual signal after cancellation.

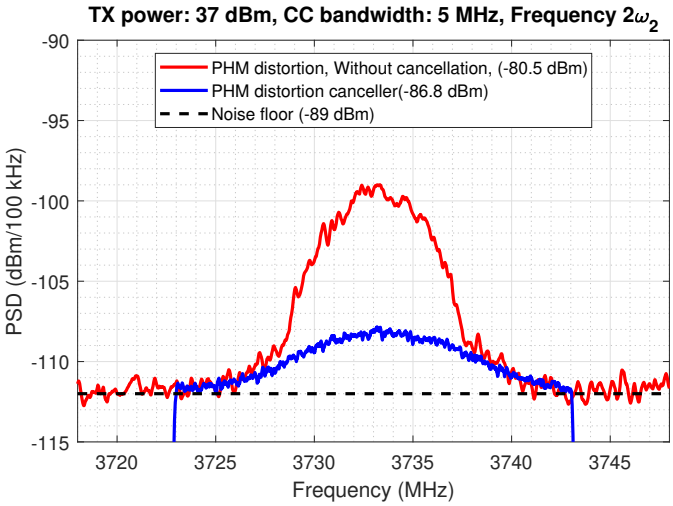

Fig. 5. The spectra of the observed PHM distortion at frequency $2\omega_2$ and the residual signal after cancellation.

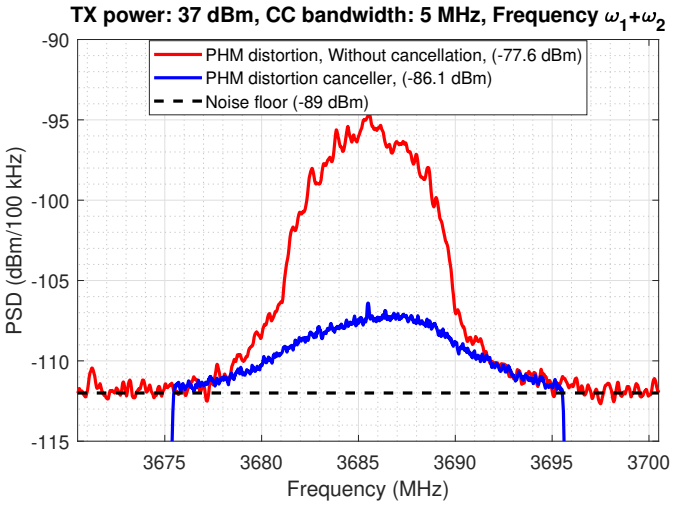

Fig. 6. The spectra of the observed PHM distortion at frequency $\omega_1 + \omega_2$ and the residual signal after cancellation.

total of 27 BFs as a concrete example. Similarly, the BFs for other even-order harmonics such as $\omega_1 + \omega_2$, and $2\omega_2$ are also illustrated in Table I.

B. Measurement Results

In this section the performance of the proposed digital cancellation method is evaluated. The observable PHM distortion products appearing at the 5G NR band n78 RX are illustrated in Fig. 3.

Next, the actual cancellation results achieved for all these fundamental harmonic distortion products are shown. For example, Fig. 4 shows the cancellation results for the frequency $2\omega_1$ where the PHM distortion power is about $6.3\,$dB above the thermal noise floor, and the cancellation achieved with the proposed cancellation method is about $5.4\,$dB using a polynomial order of $P = 4$. Hence, the residual distortion is only some $0.9\,$dB above the noise floor.

Similarly, the cancellation results for the frequency $2\omega_2$ with polynomial order of $P = 4$ are shown in Fig. 5, where the original PHM distortion power is about $8.5\,$dB, relative to the noise floor, and the achieved cancellation gain is $6.2\,$dB.

Finally, Fig. 6 shows the cancellation results achieved for frequency $\omega_1 + \omega_2$ with a polynomial order of $P = 4$. The original PHM distortion power observed here is about $11.2\,$dB, when again referenced to the thermal noise floor, while the achieved cancellation gain is $8.6\,$dB. These results demonstrate that the proposed digital cancellation method can cancel the fundamental PHM distortion products quite efficiently, thus enabling the utilization of the RF Spectrum efficiently in LTE-advanced and the 5G NR radio networks with collocated radio transceivers.

IV. Conclusion

In this paper, we proposed a novel digital cancellation solution for dealing with air-induced passive harmonic distortion in

FDD transceivers and other collocation scenarios with simultaneously active transmitters and receivers. The air-induced PHM distortion stems from the built environment close to the transceiver antenna system, that can be a serious problem in simultaneous transmit-receive systems with certain band and carrier combinations and coexisting scenarios. Behavioral models of the air-induced PHM distortion were derived and a corresponding linear-in-parameters digital canceller scheme was proposed. The performance of the proposed digital canceller was tested with actual RF measurements in an example case with coexistence of 5G NR bands n3 and n78. The air-induced PHM distortion was successfully cancelled, by up to around 9 dB in the measurements. Our future work will consider extending the cancellation solutions such that both passive harmonic and intermodulation distortion products can be efficiently modelled and suppressed.

ACKNOWLEDGMENT

This work was funded in part by the Academy of Finland (under the projects #319994, #338224, and #332361), and in part by Nokia Corporation.

REFERENCES

[1] 3GPP, "Base station (bs) radio transmission and reception," *Technical Specification (TS)*, vol. 36, pp. v8–2, 2008.

[2] A. Kiayani, V. Lehtinen, L. Anttila, T. Lahteensuo, and M. Valkama, "Linearity challenges of lte-advanced mobile transmitters: Requirements and potential solutions," *IEEE Communications Magazine*, vol. 55, no. 6, pp. 170–179, 2017.

[3] S. A. Bassam, W. Chen, M. Helaoui, and F. M. Ghannouchi, "Transmitter architecture for ca: Carrier aggregation in lte-advanced systems," *IEEE Microwave Magazine*, vol. 14, no. 5, pp. 78–86, 2013.

[4] C. S. Park, L. Sundström, A. Wallén, and A. Khayrallah, "Carrier aggregation for lte-advanced: design challenges of terminals," *IEEE Communications Magazine*, vol. 51, no. 12, pp. 76–84, 2013.

[5] V. Lampu, L. Anttila, M. Turunen, M. Fleischer, J. Hellmann, and M. Valkama, "Air-Induced PIM Cancellation in FDD MIMO Transceivers," *IEEE Microwave and Wireless Components Letters*, vol. 32, no. 6, pp. 780–783, 2022.

[6] "LTE; evolved universal terrestrial radio access (E-UTRA); user equipment (UE) radio transmission and reception (3GPP TS 36.101, version 14.1.0, release 14)," ETSI, Sophia Antipolis Cedex, France, Sep. 2016.

[7] "LTE-advanced dual uplink inter-band carrier aggregation (CA) (3GPP TS 36.860, version 13.0.0, release 13)," ETSI, Sophia Antipolis Cedex, France, Jan. 2016.

[8] M. Z. Waheed, D. Korpi, A. Kiayani, L. Anttila, and M. Valkama, "Digital self-interference cancellation in inter-band carrier aggregation transceivers: Algorithm and digital implementation perspectives," in *2017 IEEE International Workshop on Signal Processing Systems (SiPS)*, 2017, pp. 1–5.

[9] M. Zeeshan Waheed, P. P. Campo, D. Korpi, A. Kiayani, L. Anttila, and M. Valkama, "Digital cancellation of passive intermodulation in fdd transceivers," *arXiv e-prints*, pp. arXiv–1812, 2018.

[10] H.-T. Dabag, H. Gheidi, S. Farsi, P. S. Gudem, and P. M. Asbeck, "All-digital cancellation technique to mitigate receiver desensitization in uplink carrier aggregation in cellular handsets," *IEEE Transactions on Microwave Theory and Techniques*, vol. 61, no. 12, pp. 4754–4765, 2013.

[11] M. Z. Waheed, D. Korpi, L. Anttila, A. Kiayani, M. Kosunen, K. Stadius, P. P. Campo, M. Turunen, M. Allén, J. Ryynänen, and M. Valkama, "Passive intermodulation in simultaneous transmit–receive systems: Modeling and digital cancellation methods," *IEEE Transactions on Microwave Theory and Techniques*, vol. 68, no. 9, pp. 3633–3652, 2020.

[12] M. Z. Waheed, P. P. Campo, D. Korpi, A. Kiayani, L. Anttila, and M. Valkama, "Digital cancellation of passive intermodulation in fdd transceivers," in *2018 52nd Asilomar Conference on Signals, Systems, and Computers*, 2018, pp. 1375–1381.